QUASI-STATIC INDENTATION AND COMPRESSION AFTER IMPACT DAMAGE GROWTH MONITORING USING MICROFOCUS X-RAY COMPUTED TOMOGRAPHY

D.J. Bull[1*], S.M. Spearing[1], I. Sinclair[1]
[1] Faculty of Engineering and the Environment, University of Southampton, Southampton, UK
* Corresponding author (daniel.bull@soton.ac.uk)

Keywords: *damage propagation, quasi-static indentation, impact, compression after impact, carbon fibre, computed tomography, barely visible impact damage*

1 Introduction

The susceptibility of carbon fibre-polymer matrix composites to low velocity impact damage has a direct effect on the residual in-plane compressive strength [1]. Whilst the general understanding of damage caused by impact and post-impact compression is understood from studying failed specimens, the damage evolution process is still not well understood. This is largely due to the difficulty in assessing the chronology of failure processes in a high resolution, non-destructive manner. C-scans typically only capture 2D delaminations, and cross-sectional microscopy destroys the coupon and preventing the opportunity for further testing.

The use of computed tomography (CT) for step-wise series indentation experiments in composites demonstrates the feasibility of this technique for understanding damage initiation and propagation [2]. The feasibility of locally scanning full ASTM D7136M standard coupons is demonstrated in another study [3]. The use of step-wise experiments serves a purpose for ensuring finite element models are capturing the correct damage mechanisms when predicting failure loads; underpinning the predictions of these models [4].

For interpreting the damage events during low velocity impact, quasi-static indentation allows damage initiation and propagation to be monitored using CT as a function of the out-of-plane displacement. Whilst this study neglects the strain-rate behaviour of a low velocity impact test, previous studies have demonstrated similar damage and mechanical behaviours between the two techniques [5, 6].

In compression after impact tests, assessment of failed specimens typically shows failure through localized buckling. However the damage mechanisms prior to the point of critical failure are still not well understood [7].

In this study interrupted quasi-static indentation and post-impacted compression tests were performed at incremental load steps with CT performed at each step allowing non-destructive, three-dimensional damage assessments to be carried out. Preliminary results from these experiments are reported in this paper.

2 Materials and Methods

2.1 Materials

Two propriety carbon fibre prepreg systems were used in this study. These consisted of toughened systems containing particles introduced into the resin present at the interface layers and an untoughened system without particles. Intermediate modulus fibres were used. $[45/0/-45/90]_{3S}$ layups were used to form coupons measuring 150 x 100 x ~4.6 mm.

2.2 Quasi-static indentation

Coupons were placed in a universal testing machine on a base plate with a rectangular 125 x 75 mm

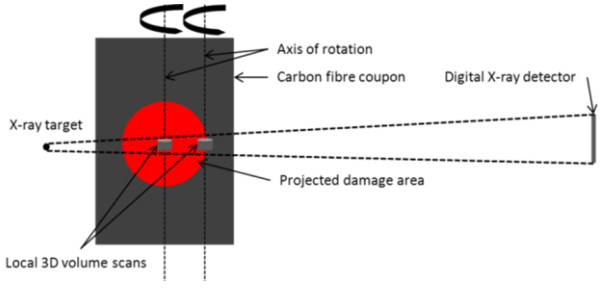

Fig 1. Schematic of CT scan setup

window. The testing machine had the capability of recording the load-displacement curve for the loading cycle only. A 16 mm diameter hemispherical tup applied an out-of-plane displacement to the centre of the coupon; tests were interrupted after a displacement of 2 mm, 2.5 mm, 3 mm, 4 mm and 5 mm were applied. To achieve this, at each increment the tup was positioned so it made contact with the coupon followed by the respective displacements. To take into account the indentation, i.e. the tup not being in line with the plane on of the non-indented surface, the dent depth was measured after each applied load. The true displacement on each coupon added together the dent depth from the previous load to the displacement applied by the machine.

Interruptions to the tests allowed ultrasonic C-scans and CT scans to take place, allowing for monitoring of damage imitation and growth.

2.3 Compression after impact

Coupons were impacted according to ASTM D7136M standards using a 16 mm hemispherical tup with a mass of 4.9 kg. Coupons were impacted at 25 J and 30 J for the untoughened and toughened coupons respectively. A lower impact energy was chosen for the untoughened system to enable the majority of damage to be within the field of view of the CT scan. Coupons were CT scanned after impact and following application of incremental load steps near the critical failure load. The first load was applied to two standard deviations below the mean failure load based on previous mechanical testing results. Subsequent loads were incremented at approximately 2 kN load steps or until audible damage was heard.

Loads were normalized to the failure load. In the toughened system the near failure load reached 103% of the failure load whereas the toughened system reached 99%.

2.4 Microfocus computed tomography

CT scans were undertaken at the µ-VIS CT facility at the University of Southampton, UK[1].

Coupons were stacked upright in pairs and CT scanned at a voxel resolution of 14.3µm. A schematic of the setup used for the CT scan is shown in Fig. 1. The specimen was positioned so there was marginal clearance (~5 mm) between the edge of the coupons and the X-ray target. The distance between the coupon and the target limited the maximum voxel resolution with this setup. Two coupons were scanned together to maximize the field of view in the local scan and to increase scanning throughput.

A fast acquisition time of 45 minutes was used; this further increased the throughput of coupons that could be scanned whilst maintaining a good balance of low noise in the scan. Coupons were scanned with the following settings: 115 kV (peak) ~40 kV (mean), 100 µm, 1000 ms exposure time, two frames per projection and 1301 radiographs across 360° of rotation.

For the *ex situ* compression after impact loading, two local regions of interest were scanned; one at the impact point, and the other at the edge of the damaged region, determined from C-scans. For *ex situ* quasi-static indentation, a local region at the contact point was scanned at each displacement level.

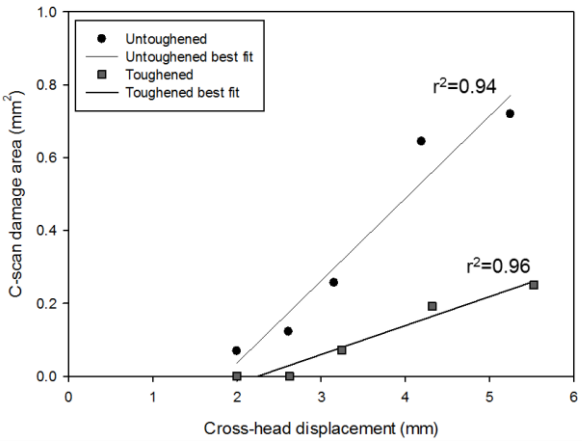

Fig 2. Plot of projected damage area against out of plane displacement for both untoughened and toughened systems.

3 Results and discussion

3.1 Interrupted quasi-static indentation tests

[1] µ-VIS: Multidisciplinary, Multiscale, Microtomographic Volume Imaging, www.soton.ac.uk/muvis

Comparisons between the normalized projected damage areas are shown in Fig. 2. In both material systems there is an approximately linear trend of projected damage area to the out-of-plane displacement.

It is clear the toughened system suppresses the damage area. This is shown by a lower gradient in the best-fit line of the toughened system compared to the untoughened system. This enabled the projected damage area to be lower by a factor of approximately four across the range of displacements tested.

The load displacement plots for each material system at each of the incremental loading cycles are plotted in Fig. 3. These are compared against the initiation and growth of damage shown in the CT cross-sections shown in Fig. 4. at the contact region.

Cross-sectional slices (Fig. 4.) of an untoughened and toughened system show damage initiation and growth at incremental quasi-static indentation

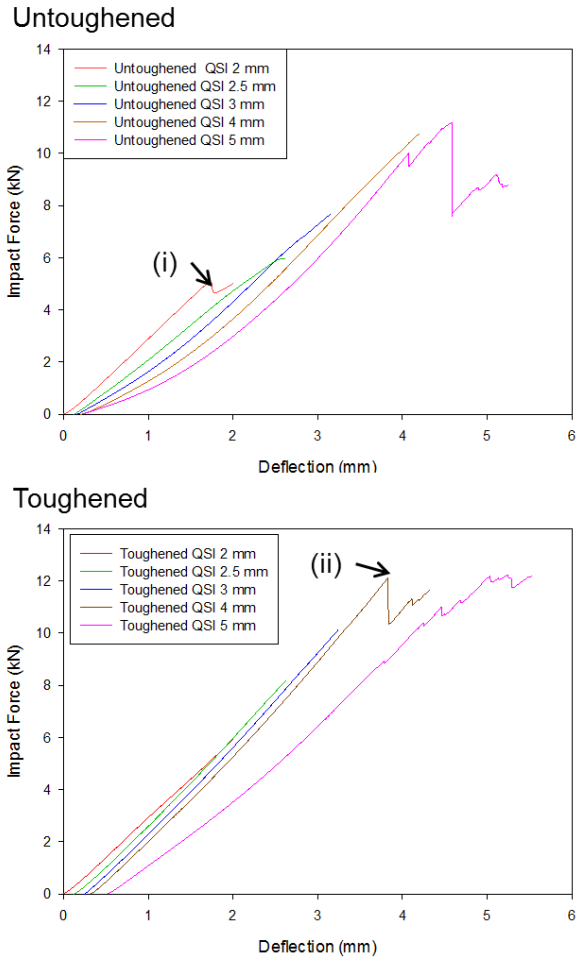

Fig 3. Load-displacement plots for the untoughened and toughened coupons at each incremental displacement.

displacements on a toughened coupon. Damage mechanisms were observed on both the untoughened and toughened system consisting of (i) matrix cracks, (ii) tensile cracks at the back face, (iii) delaminations and (iv) fibre fracture.

The sequence of damage events were captured in the toughened system as the coupon was incrementally displaced. Tensile cracks were first observed occurring on the back face. These were followed by matrix crack that were dominantly present below mid-plane. These matrix cracks led to delaminations which are shown to open more at higher displacements. Finally fibre fracture was observed occurring below mid-plane directly in line with the contact point.

Interestingly, bridging ligaments were visible in the CT scans circled in (v). Such bridging ligaments toughen the material at the interface through crack tip shielding processes. These bridging ligaments were subsequently not observed at the highest displacement suggesting these mechanisms have failed resulting in a more open crack in the wake and an advancement of the crack.

Studying the force-displacement curve in Fig. 3., a load drop was observed in the untoughened system at ~1.9 mm (i) corresponding to the onset of damage. The extent of damage in the untoughened system at 2 mm is visually quite extensive as shown in C-scan data in Fig. 2. and CT cross-sections in Fig. 4. This suggests the possibility that damage may have occurred suddenly at this critical load. In contrast, the toughened system exhibited a more progressive damage formation in the toughened system which correlated with some non-linearity in the force-displacement curve. One possible explanation for the progressive damage formation is crack bridging and ductility in the toughened system in contrast to the brittle untoughened system.

At the highest displacements, a load drop is observed in both the untoughened and toughened systems. This corresponded to fibre fracture Fig. 3. (ii) first initiating at 4 and 5 mm displacements for the toughened and untoughened systems respectively. Despite the toughened system suppressing the projected damage area by a factor of four, an abundance of fibre fracture occurred at a lower displacement level compared to the untoughend system. This similar behaviour was also

observed in [8]. It is likely that delaminations in the untoughened system relieved the stresses leading to fibre fracture, subsequently delaying the onset of this behaviour. Such fibre fracture will have a direct effect on the residual tensile strength, and may be a trade-off with toughened systems. This suggests further work into the effects of residual tensile strength after impact across different toughened systems.

It should be highlighted that one weakness of the interrupted quasi-static indentation technique is the cyclic loading and unloading of the coupons. This may have led to a contribution of fatigue to damage growth. Nonetheless the evolution of damage growth was captured progressively. Development of *in situ* experiments in future could potentially remove this weakness in addition to monitoring the behaviour of cracks whilst under a load.

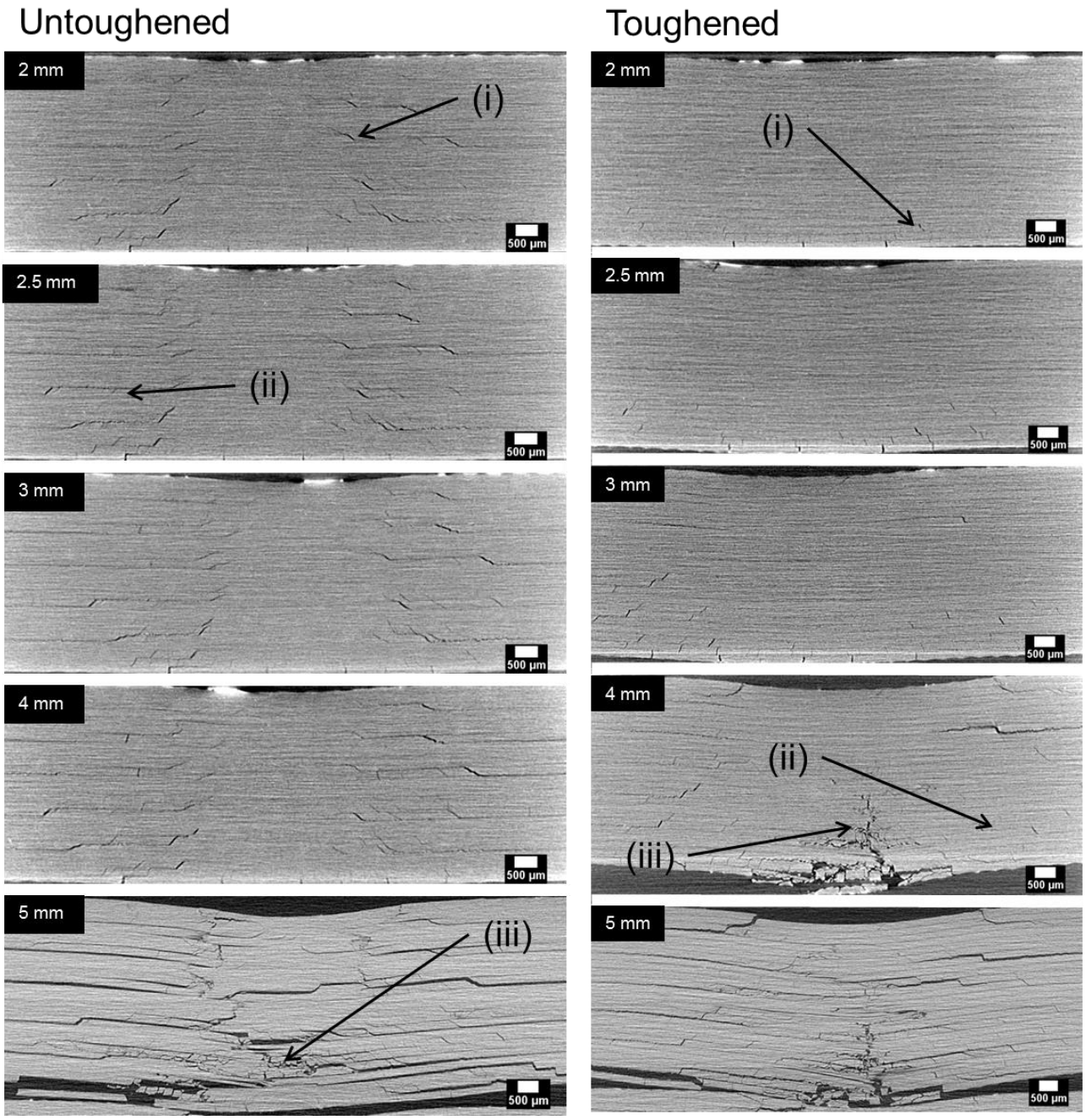

Fig 4. CT cross-sections showing initiation and propagation of damage at increasing out-of-plane displacements.

3.2 Interrupted compression after impact tests

A CT cross-section of damage at the impact region of an untoughened coupon is shown in Fig. 5. after impact and after application of a near failure load. In the untoughened system, some delamination growth was observed after application of near failure loads within the cone of damage at the impact site (i). In addition to this, crack openings were shown to increase at the near surface plies after application of near failure loads, circled in (ii). This likely explains the blistering effects observed in other studies [9]. The toughened system did not show these characteristics as no observable damage growth was detected; however, studies of lower damage resistant particle toughened systems did reveal the presence of these characteristics. The lack of detectable damage prior to failure could explain why the toughened system failed with a higher load to near failure load in comparison with the untoughened system that exhibited damage growth at near failure load and subsequently failed with a lower load.

The presence of preexisting 0° fibre fracture in one of the particle toughened systems was shown to grow laterally across the ply at near failure loads. This behaviour is shown in Fig. 6. In systems were no 0° fibre fracture was present after impact, there was no detectable fibre fracture at near failure loads. It is likely the failed fibres led to a redistribution of load to the neighbouring 0° load bearing fibres leading to further fibre fracture.

Fig. 7. shows a 3D segmentation of delamination damage between two ply interfaces surrounding a 90° ply four plies in from the impact. This was captured on another particle system with lower toughness. It shows that where delamination growth was present, this typically occurred only within the cone of damage beneath the impact site between the interfaces containing 90° plies (i). This damage occurred on the upper ply interface and was constrained by the two 90° matrix cracks growing laterally across the width of the coupon. No observable delamination growth was observed in the 45° ‘wedge’ of delamination (ii), however the extent of bridging behaviour in delaminations is reduced. This reduction in bridging is shown (iii) where interconnectivity is observed in this region by discontinuities in the delamination in the unloaded stage. After application of a near failure load interconnectivity is reduced in the near failure stage.

There is the possibility that bridging creates traction sites between ply interfaces leading to an increase in stability of sublaminates by offering reinforcement in the Z-direction, similarly to Z-pinning or stitching [10, 11]. This is in addition to bridging behaviour acting to shield the crack tip reducing stresses and subsequently hindering the propagation of crack growth.

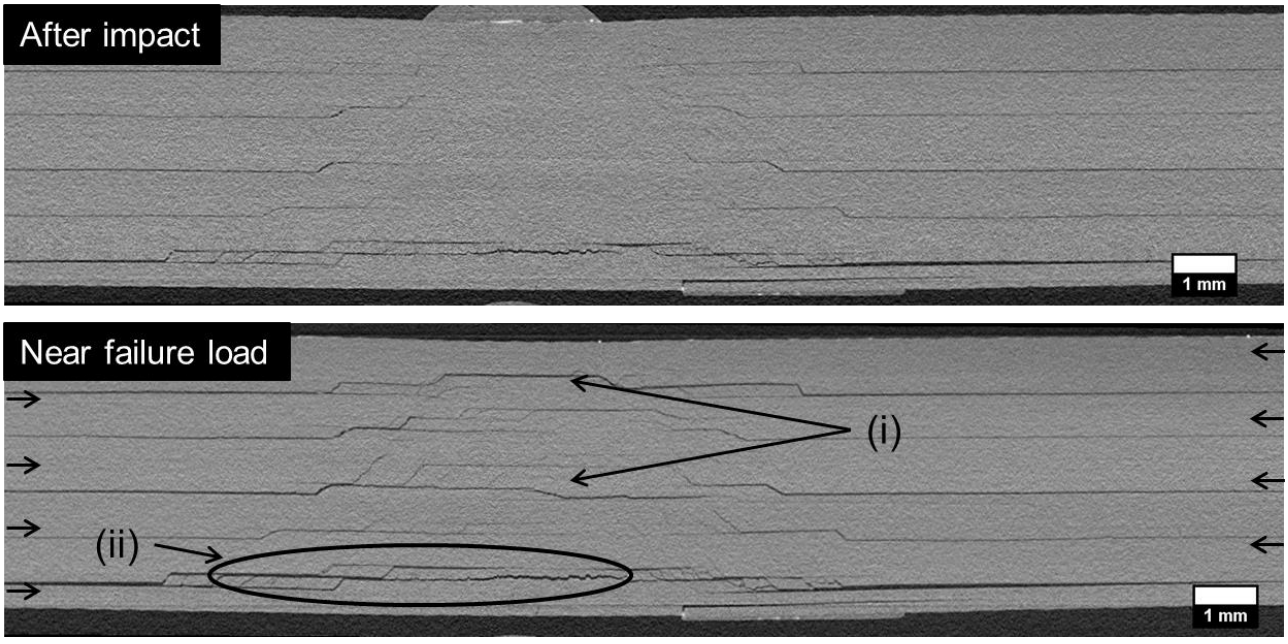

Fig 5. CT cross-section of the untoughened coupon showing damage after impact and after application of a near failure in-plane compression load. Arrows indicate the direction of loading.

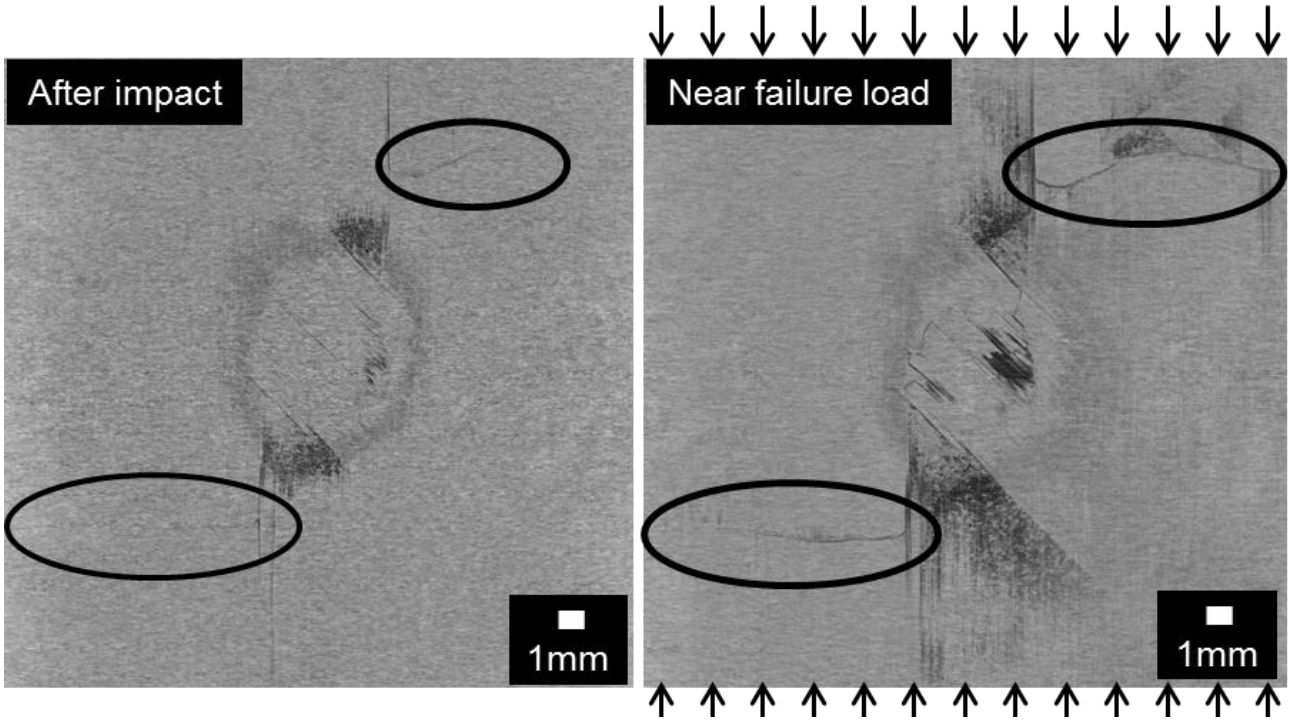

Fig 6. CT cross-section parallel to crack front in a toughened system. Circled is fibre fracture on the load bearing 0° plies which has grown laterally after application of near failure load. Arrows indicate direction of loading.

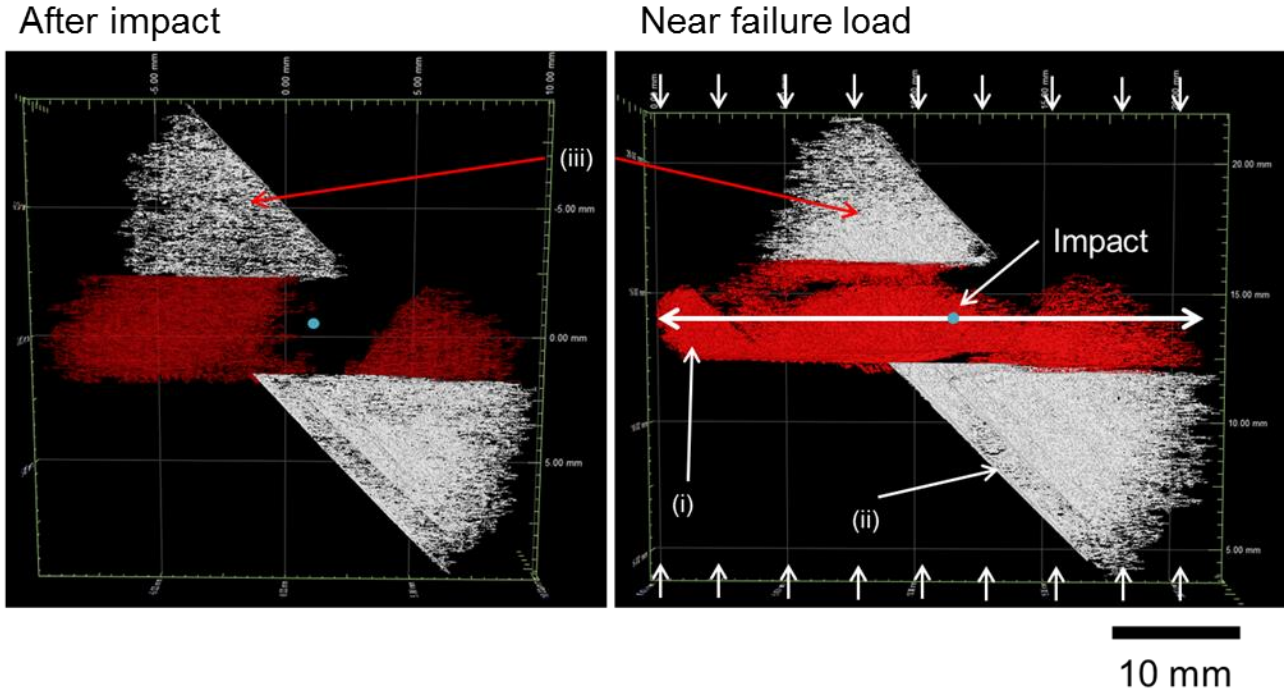

Fig 7. 3D segmentation of delamination in a particle toughened system. Arrows indicate in-plane loading direction. (i) delamination growth propagating laterally, (ii) 45° delamination wedge, (iii) bridging behaviour which is reduced after application of near failure load.

Whilst both the toughened and untoughened materials failed in compression suddenly, there was a build-up of audible noise prior to failure in the toughened system whereas the untoughened system failed without this behaviour. This noise could have been contributed by failure of the bridging ligaments at the near failure and final failure load as little damage growth was detected at the regions scanned.

It is possible the compression strength of the particle systems is limited by the failure strength of the bridging sites under application of an in-plane load in conjunction with the size of the damage area. When these sites failed, a loss in traction and an increase to the unsupported length of the delamination could contribute to final failure of the coupon. The possibility of bridging sites serving a secondary role after impact for increasing the residual compressive strength is interesting and could be implemented into finite element models to more accurately predict failure. This can be achieved by applying cohesive zones to delaminations.

Fig. 8. shows a CT cross-section of the toughened coupon failed in compression. Sublaminates typically four plies thick (i) are shown to fail by shear buckling as suggested by the angle of the fracture, e.g. near (ii). Buckling sites of the sublaminates fracture along the pre-existing 90° matrix cracks induced by impact, circled in (ii), and was observed across all the other systems studied. The buckling failure at these matrix crack sites is of interest and may be contributed by higher stresses at the transition point between the matrix crack and delamination in the sublaminate when under load. It is commonly agreed that delaminations contribute most significantly to compressive failure [12, 13] however, matrix cracks may also have a significant contribution towards compressive failure than first thought. Inclusion of 90° matrix cracks into finite element models may yield more accurate results regarding predicting final failure loads.

4 Further work

Whilst preliminary results from quasi-static indentation tests enabled the progression of damage to be monitored, its viability as a method of replicating low velocity impact events are still open to debate. A comparison between coupons subjected to quasi-static indentation and low velocity impact would enable better understanding of the similarities and differences between the two loading conditions.

The feasibility of Synchrotron Radiation Computed Laminography has enabled sub-micron voxel resolution 3D imaging on carbon fibre coupons [14, 15]. A combination of this imaging technique with *ex situ* quasi-static indentation will enable the initiation and propagation of damage micromechanisms to be studied in better detail. This will help better understand the role of particle toughening.

Preliminary work studied the damage from CT data

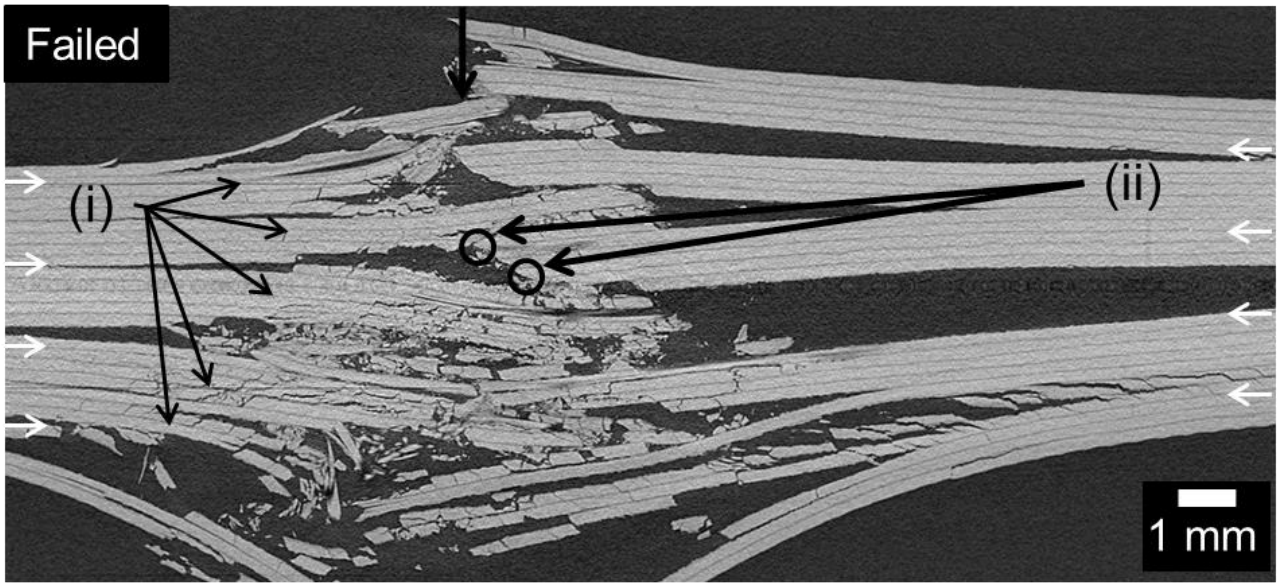

Fig 8. CT cross-section of particle toughened system failed in compression. Arrows indicate the direction of in-plane loading.

qualitatively. Quantitative measurement of the distribution of damage areas would be useful for validating finite element models and additionally be useful for toughening strategies where toughening is directed to certain ply interfaces.

The study of *ex situ* compression after impact showed cracks were opening near the impact site at near failure loads. These can be quantified using partial volume correction techniques [16]. One weakness of the *ex situ* compression after impact test was the cyclic loading/unloading in the test. Further work would be required to develop an in situ rig capable of imaging the coupon under load; this will also enable cracks to be held open during load.

The observation of buckling failure along pre-existing 90° matrix cracks suggests finite element models should incorporate this crack into models.

5 Conclusions

Microfocus CT is shown to work well for non-destructive observations of composite damage growth in time-series experiments. Quasi-static indentation showed the initiation of matrix cracks followed by delaminations and finally fibre fracture. The location of damage was shown to initiate below mid-plane on the toughened coupon starting with matrix cracks which led to delamination formation. Delamination damage was progressive in the toughened system compared to the untoughened coupon where the onset of damage corresponded to a sudden load drop in the force-displacement curve. Whilst toughened systems suppress damage growth, the onset of fibre fracture occurred at a lower displacement compared to the untoughened system. This is a potential trade-off with toughened systems as fibre fracture will affect the residual tensile strength.

In post-impact compression tests, some delamination growth was observed at near failure loads in the untoughened and particle toughened systems with lower damage resistance. Delamination growth typically existed within the cone of damage beneath the impact site. Larger crack openings were observed at the near surface plies at the impact site. CT scans of failed compression after impact coupons showed shear buckling failure of the delaminated sublaminates. These sublaminates buckle in groups of approximately four plies and commonly occur along the preexisting 90° matrix crack sites. .

Acknowledgements

Thanks to the EPSRC and Cytec engineered materials Ltd for sponsorship of this work. Particular thanks go to Dr. Kingsley Ho at Cytec for his contribution as a technical point of contact. The mu-vis centre at the University of Southampton, UK, is acknowledged for providing the facilities that made this work possible. Thanks Dr. Anna Scott for providing help with µCT scanning.

References

[1] P.A. Lagace, J.E. Williamson, P.H.W. Tsang, E. Wolf and S. Thomas, "A Preliminary Proposition for a Test Method to Measure (Impact) Damage Resistance", *J Reinf Plast Comp*, Vol. 12, No. 5, pp 584-601, 1993.

[2] J.Y. Buffiere, E. Maire, J. Adrien, J.P. Masse and E. Boller, "In Situ Experiments with X ray Tomography: an Attractive Tool for Experimental Mechanics", *Exp Mech*, Vol. 50, No. 3, pp 289-305, 2010.

[3] D.J. Bull, L. Helfen, I. Sinclair, S.M. Spearing and T. Baumbach, "A comparison of multi-scale 3D X-ray tomographic inspection techniques for assessing carbon fibre composite impact damage", *Compos Sci Technol*, Vol. 75, No., pp 55-61, 2013.

[4] P. Wright, A. Moffat, I. Sinclair and S.M. Spearing, "High resolution tomographic imaging and modelling of notch tip damage in a laminated composite", *Compos Sci Technol*, Vol. 70, No. 10, pp 1444-52, 2010.

[5] R. Olsson, "Mass criterion for wave controlled impact response of composite plates (vol 31, pg 879, 2000)", *Compos Part a-Appl S*, Vol. 32, No. 2, pp 291-, 2001.

[6] S.R. Swanson, "Limits of Quasi-Static Solutions in Impact of Composite Structures", *Compos Eng*, Vol. 2, No. 4, pp 261-7, 1992.

[7] K.D. Challenger, "The Damage Tolerance of Carbon-Fiber Reinforced Composites - a Workshop Summary", *Compos Struct*, Vol. 6, No. 4, pp 295-318, 1986.

[8] K.T. Tan, A. Yoshimura, N. Watanabe, Y. Iwahori and T. Ishikawa, "Effect of stitch density and stitch thread thickness on damage progression and failure characteristics of stitched composites

under out-of-plane loading", *Compos Sci Technol*, Vol. 74, No. 24, pp 194-204, 2013.
[9] F.A. Habib, "A new method for evaluating the residual compression strength of composites after impact", *Compos Struct*, Vol. 53, No. 3, pp 309-16, 2001.
[10] X. Zhang, L. Hounslow and M. Grassi, "Improvement of low-velocity impact and compression-after-impact performance by z-fibre pinning", *Compos Sci Technol*, Vol. 66, No. 15, pp 2785-94, 2006.
[11] A.P. Mouritz, "Review of z-pinned composite laminates", *Compos Part a-Appl S*, Vol. 38, No. 12, pp 2383-97, 2007.
[12] M. de Freitas and L. Reis, "Failure mechanisms on composite specimens subjected to compression after impact", *Compos Struct*, Vol. 42, No. 4, pp 365-73, 1998.
[13] G.J. Williams, I.P. Bond and R.S. Trask, "Compression after impact assessment of self-healing CFRP", *Compos Part a-Appl S*, Vol. 40, No. 9, pp 1399-406, 2009.
[14] L. Helfen, T. Baumbach, P. Mikulik, D. Kiel, P. Pernot, P. Cloetens, et al., "High-resolution three-dimensional imaging of flat objects by synchrotron-radiation computed laminography", *Appl Phys Lett*, Vol. 86, No. 7, pp 071915, 2005.
[15] A.J. Moffat, P. Wright, L. Helfen, T. Baumbach, G. Johnson, S.M. Spearing, et al., "In situ synchrotron computed laminography of damage in carbon fibre-epoxy [90/0](s) laminates", *Scripta Mater*, Vol. 62, No. 2, pp 97-100, 2010.
[16] D.J. Bull, I. Sinclair and S.M. Spearing, "Partial volume correction for approximating crack opening displacements in CFRP material obtained from micro-focus X-ray CT scans", *Compos Sci Technol*, In press, 2013.